J|A|C|S ARTICLES

Published on Web 07/21/2009

Protonated Benzene Dimer: An Experimental and Ab Initio Study

Shamik Chakraborty,[†,§] Reza Omidyan,[†,||] Ivan Alata,[†] Iben B. Nielsen,[†] Claude Dedonder,[†,‡] Michel Broquier,[†,‡] and Christophe Jouvet*[,†,‡]

Centre Laser de l'Université Paris Sud (EA. 4127), Bât. 106, Univ. Paris-Sud 11 - 91405 Orsay Cedex, France, and Laboratoire de Photophysique Moléculaire du CNRS (UPR 3361), Bât. 210, Univ. Paris-Sud 11 - 91405 Orsay Cedex, France

Received April 21, 2009; E-mail: christophe.jouvet@u-psud.fr

Abstract: The excitation spectrum of the protonated benzene dimer has been recorded in the 415−600 nm wavelength range. In contrast to the neutral iso-electronic benzene dimer, its absorption spectrum extends in the visible spectral region. This huge spectral shift has been interpreted with ab initio calculations, which indicate that the first excited states should be charge transfer states.

Introduction

The characterization of structure, dynamics, and electronic properties of protonated molecules, mainly organic molecules, is of fundamental interest in physical organic chemistry. This transient species is important to study for understanding the dynamics and selectivity of chemical processes. Protonated aromatic molecules (AH^+) are commonly recognized as the intermediates in electrophilic aromatic substitution reactions (EAS),[1] one of the most commonly encountered reaction mechanisms in organic chemistry.[2] Molecular level understanding of the mechanistic details of EAS type of reactions solely depends on characterization of AH^+ species. Protonated aromatic molecules play a role as short-lived intermediates in a broad variety of environments, from astrochemistry and organic chemistry to hydrocarbon plasma (e.g., flame combustion),[3−5] engine gas exhaust,[6] and biophysics. The effects of protonation on aromatic biomolecules is an interesting issue for models rationalizing the UV photostability of biological macromolecules, such as proteins and DNA.[7−11]

Although these species are important intermediates, little is known[12,13] about their geometric and electronic structure, reactivity, and dynamics, even for simple isolated AH^+ ions. Recent developments of efficient ion sources, ion trapping techniques, and sensitive IR spectroscopic detection have stimulated substantial progress in the characterization of the geometric structure of isolated and microsolvated AH^+ ions in the gas phase. High-resolution IR lasers coupled with supersonic expansion techniques and different ion sources make it possible to record high-resolution IR spectra of cold protonated aromatic molecules in their ground electronic state.[14−20]

If the information on excited states of protonated molecules is sparse, even less is known on excited states of protonated clusters. To our knowledge, the only experiment reported at present is the experiment of Mercier et al.[21] where it has been shown that complexation with two water molecules induces a considerable lengthening of the very short lifetime of free protonated tryptophan from the femtosecond time scale to the picosecond range. This effect has been explained by a quite general process, which needs to be studied in detail: as in many aromatic protonated species, a low lying excited state corresponding to the transfer of an electron from the aromatic ring

[†] Centre Laser de l'Université Paris Sud.
[‡] Laboratoire de Photophysique Moléculaire du CNRS.
[§] Present address: Institut fuer Optik and Atomare Physik, Technische Universitaet Berlin, Hardenbergstrasse 36 D-10623, Berlin, Germany.
[||] Present address: Department of Chemistry, Isfahan University of Technologhy, Isfahan 84154, Iran.

(1) Olah, G. A. *Acc. Chem. Res.* **1971**, *4*, 240.
(2) Smith, M. B.; March, J. *Advanced Organic Chemistry: Reactions, Mechanisms, and Structure*, 5th ed.; Wiley: New York, 2001.
(3) Pasquiers, S. *Eur. Phys. J.: Appl. Phys.* **2004**, *28*, 319–324.
(4) Pasquiers, S.; Postel, C.; Magne, L.; Puech, V.; Lombardi, G. *J. Adv. Oxid. Technol.* **2004**, *7*, 108–115.
(5) Magne, L.; Pasquiers, S.; Blin-Simiand, N.; Postel, C. *J. Phys. D: Appl. Phys.* **2007**, *40*, 3112–3127.
(6) Kiendler, A.; Arnold, F. *Atmos. Environ.* **2002**, *36*, 2979–2984.
(7) Kang, H.; Jouvet, C.; Dedonder-Lardeux, C.; Martrenchard, S.; Charriere, C.; Gregoire, G.; Desfrancois, C.; Schermann, J. P.; Barat, M.; Fayeton, J. A. *J. Chem. Phys.* **2005**, *122*, 084307.
(8) Kang, H.; Jouvet, C.; Dedonder-Lardeux, C.; Martrenchard, S.; Gregoire, G.; Desfrancois, C.; Schermann, J. P.; Barat, M.; Fayeton, J. A. *Phys. Chem. Chem. Phys.* **2005**, *7*, 394–398.
(9) Boyarkin, O. V.; Mercier, S. R.; Kamariotis, A.; Rizzo, T. R. *J. Am. Chem. Soc.* **2006**, *128*, 2816–2817.
(10) Gregoire, G.; Dedonder-Lardeux, C.; Jouvet, C.; Desfrancois, C.; Fayeton, J. A. *Phys. Chem. Chem. Phys.* **2007**, *9*, 78–82.
(11) Fujihara, A.; Matsumoto, H.; Shibata, Y.; Ishikawa, H.; Fuke, K. *J. Phys. Chem. A* **2008**, *112*, 1457–1463.
(12) Freiser, B. S.; Beauchamp, J. L. *J. Am. Chem. Soc.* **1976**, *98*, 3136–3139.
(13) Freiser, B. S.; Beauchamp, J. L. *J. Am. Chem. Soc.* **1977**, *99*, 3214–3225.
(14) Hudgins, D. M.; Bauschlicher, C. W.; Allamandola, L. J. *Spectrochim. Acta, Part A: Mol. Biomol. Spectrosc.* **2001**, *57*, 907–930.
(15) Solcà, N.; Dopfer, O. *Angew. Chem., Int. Ed.* **2002**, *41*, 3628–3631.
(16) Dopfer, O. *Int. Rev. Phys. Chem.* **2003**, *22*, 437.
(17) Solca, N.; Dopfer, O. *J. Chem. Phys.* **2004**, *120*, 10470–10482.
(18) Dopfer, O. *J. Phys. Org. Chem.* **2006**, *19*, 540–551.
(19) Lorenz, U. J.; Solca, N.; Lemaire, J.; Maitre, P.; Dopfer, O. *Angew. Chem., Int. Ed.* **2007**, *46*, 6714–6716.
(20) Douberly, G. E.; Ricks, A. M.; Schleyer, P. v. R.; Duncan, M. A. *J. Phys. Chem. A* **2008**, *112*, 4869.
(21) Mercier, S. R.; Boyarkin, O. V.; A., K.; Guglielmi, M.; Tavernelli, I.; Cascella, M.; Rothlisberger, U.; Rizzo, T. R. *J. Am. Chem. Soc.* **2006**, *128*, 16938–16943.

toward the proton is present. The addition of one electron on this proton leads to the formation of a hypervalent Rydberg type structure, which should be highly unstable and leads to fast reorganization of the molecule.[22,23] In the solvation process, this Rydberg state is destabilized and pushed at higher energy, and thus the optically accessible excited state becomes more stable as observed for protonated tryptophan case with two water molecules.

Protonated molecules and clusters are iso-electronic to the neutral systems, and usually in neutral systems, the complexation process leads to very small changes in the electronic transitions (except in the case where excitation triggers a chemical reaction). We will see that complexation induces drastic change in the electronic transitions of protonated systems.

As a first study, we have investigated a simple system, the protonated benzene dimer, and we report the first observation of its excitation spectrum that is strongly perturbed as compared to the excitation spectrum of neutral benzene dimer. The neutral benzene dimer has been the subject of many investigations.[24−33] Indeed, the formation of the dimer in the neutral system has the effect of breaking the D_{6h} symmetry, which allows the S_1-S_0 origin transition to be observed. The spectral shift measured on the origin as well as on the vibronic transitions is very small as expected for a van der Waals interaction.[34−36]

In this Article, we report the S_1-S_0 electronic excitation spectrum of protonated benzene dimer (BBH^+) as compared to the benzene dimer radical cation (BB^+) spectrum in the wavelength range of 413−600 nm. Experimental results are supported by ab initio quantum chemical computations.

Experimental Details

Protonated benzene dimer and benzene dimer radical cation are produced in a pulsed high voltage electric discharge source. The electric discharge source is coupled to a pulsed nozzle (General Valve) of 200 μm diameter. Hence, ions are produced in a supersonically expanded molecular beam. Two 20 mm diameter brass plates are mounted on the valve head to achieve the discharge along the molecular beam axis. The first plate is placed 1 mm downstream from the valve orifice. A 1 mm thick Teflon spacer is placed between the valve and the first brass plate for electrical isolation. The second plate is isolated from the first one by a 3 mm thick Teflon spacer. An approximately 500 ns wide, 1000 V pulse is generated with a home-built high voltage power supply and applied on the first plate, the second plate being grounded. It produces a discharge in the middle of the 200−250 μs wide gas pulse along the molecular beam path. The gas mixture consists of 50% of He and 50% of H_2 seeded with benzene vapor (benzene from Sigma-Aldrich is used without any further purification). The buffer gas mixture is sent through the benzene kept in a container outside the chamber. Benzene has a very high vapor pressure, and its concentration during the experiment is controlled by cooling the sample container with ice−water. The typical stagnation pressure is about 2 bar. The typical working pressure in the source chamber was 1×10^{-5} mbar, and in the TOFMS chamber it was 2×10^{-6} mbar.

The expansion of produced ions in the molecular beam is collimated by a 5 mm diameter skimmer at a distance of 10 cm downstream from the nozzle orifice. The collimated ion beam is then passed into a second differentially pumped chamber.

The ions produced in the source chamber are pulsed extracted into a reflectron time-of-flight mass spectrometer. The mass spectrometer is in the perpendicular direction to the molecular beam axis. A reasonably good mass resolution is achieved with a field free time-of-flight distance of 157 cm before the channel plate detector. In this condition, two masses, $m/z = 156$ for benzene dimer radical cation (BB^+) and m/z=157 for protonated benzene dimer cation (BBH^+), are well resolved. Laser-induced photofragmentation is carried out using a 10 Hz, nanosecond OPO laser (Euroscan). The third harmonic (355 nm) of the Nd^{3+}:YAG (Quantel YG981C) laser pumps the BBO crystal of the OPO laser, delivering a tunable wavelength range of 415−670 nm with an output power in the range of 10−15 mJ.

One of the problems of this experiment is that the photofragments issued from BBH^+ are BH^+ and may be $C_6H_5^+$, which are already present in the beam (produced in the discharge source) and are extracted together with all other ions. To detect the weak photoproduct signal on top of the ion signal coming from the beam is not possible unless these ions have been removed before arriving in the region of interaction with the laser. Instead of looking at the ionic photoproduct, it is simpler to detect the neutral product as it was done to study the photodissociation of benzene cluster radical cations.[37] The scheme of the experiment is depicted in Figure 1.

The ions from the discharge are extracted and accelerated to the first field free region of the mass spectrometer by two electrodes. The voltages on these plates (~2200 and ~1800 V) are pulsed and adjusted to focus temporally the ions in the interaction region (Wiley Mac-Laren conditions) located 10 cm before the channel plate detector 1. Between the interaction region and the detector, the reflectron grids repel the ions (parent and products), which can eventually be detected on a second pair of channel plates (detector 2) after a second field free region.

The first detector is detecting all of the neutral species produced from fragmentation of accelerated ions, which includes the fragments produced by the laser and those produced by collisions with the residual gas in the field free region. To discriminate between the photoproducts and the collisional background, the laser is interacting with the ions in a region held at a fixed potential of −2 kV where the parent ions gain a kinetic energy of ~4 keV. The interaction zone is very short (2 cm) so that the number of neutral fragments produced by collision in this region is very small and can be neglected. The neutral fragments produced from the photofragmentation process will have the same velocity as their parent ions. The arrival time on detector 1 of the neutral fragments produced in the interaction region or in the field free region is presented in Figure 2. The narrow peak corresponds to the neutral particles produced in the interaction region from ions having a kinetic energy of 4 keV, whereas the broad peak corresponds to

(22) Gregoire, G.; Jouvet, C.; Dedonder, C.; Sobolewski, A. L. *Chem. Phys.* **2006**, *324*, 398–404.
(23) Gregoire, G.; Jouvet, C.; Dedonder, C.; Sobolewski, A. L. *J. Am. Chem. Soc.* **2007**, *129*, 6223–6231.
(24) Janda, K. C.; Hemminger, J. C.; Winn, J. S.; Novick, S. E.; Harris, S. J.; Klemperer, W. *J. Chem. Phys.* **1975**, *63*, 1419–1421.
(25) Hopkins, J. B.; Powers, D. E.; Smalley, R. E. *J. Phys. Chem.* **1981**, *85*, 3739–3742.
(26) Langridge-Smith, P. R. R.; Brumbaugh, D. V.; Haynam, C. A.; Levy, D. H. *J. Phys. Chem.* **1981**, *85*, 3742–3746.
(27) Fung, K. H.; Selzle, H. L.; Schlag, E. W. *J. Phys. Chem.* **1983**, *87*, 5113–5116.
(28) Law, K.; Schauer, M.; Bernstein, E. R. *J. Chem. Phys.* **1984**, *81*, 4871–4882.
(29) Henson, B. F.; Hartland, G. V.; Venturo, V. A.; Felker, P. M. *J. Chem. Phys.* **1992**, *97*, 2189–2208.
(30) Scherzer, W.; Krätzschmar, O.; Selzle, H. L.; Schlag, E. W. *Z. Naturforsch.* **1992**, *47a*, 1248–1252.
(31) Ebata, T.; Hamakado, M.; Moriyama, S.; Morioka, Y.; Ito, M. *Chem. Phys. Lett.* **1992**, *199*, 33–41.
(32) Arunan, E.; Gutowsky, H. S. *J. Chem. Phys.* **1993**, *98*, 4294–4296.
(33) Hirata, T.; Ikeda, H.; Saigusa, H. *J. Phys. Chem. A* **1999**, *103*, 1014–1024.
(34) Spirko, V.; Engvist, O.; Soldan, P.; Selzle, H. L.; Schlag, E. W.; Hobza, P. *J. Chem. Phys.* **1999**, *111*, 572–582.
(35) Sinnokrot, M. O.; Sherrill, C. D. *J. Phys. Chem. A* **2006**, *110*, 10656–10668.
(36) Dinadayalane, T. C.; Leszczynski, J. *Struct. Chem.* **2009**, *20*, 11–20.
(37) Nakai, Y.; Ohashi, K.; Nishi, N. *J. Phys. Chem. A* **1997**, *101*, 472–480.

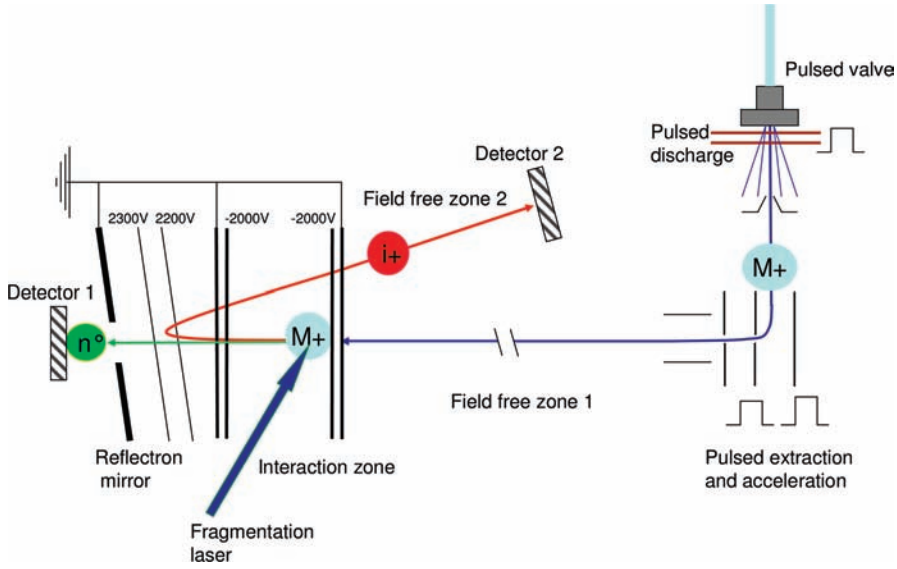

Figure 1. Scheme of the experimental setup: the ions are formed in an electric discharge located just after the pulsed valve generating the supersonic expansion. The jet is skimmed, and the parent ions are extracted and accelerated with pulsed voltages and enter a first field free region. They enter the interaction zone located just in front of the electrostatic reflector where they are excited with the laser and photofragmented. The ions are selected by their arrival time in the interaction region. The interaction zone is held at a fixed potential so that the neutral fragments have a sufficient kinetic energy to be detected efficiently on detector 1 and differentiated from collision-induced fragments. The unfragmented parent ions can be reflected and detected after the second field free region on a second microchannel plate detector 2.

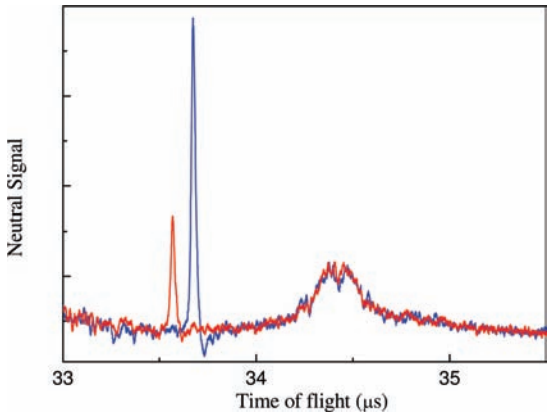

Figure 2. Time of flight spectra of the neutral fragments arriving on detector 1: in the red trace, the laser delay is adjusted to dissociate the BB^+ ions; for the blue trace, the delay is fixed to dissociate the BBH^+ ions. The broad peak corresponds to collision-induced dissociations.

collision-induced neutral fragments produced in the long field free region from ions having a kinetic energy of 2 keV. Hence, the neutral particles produced in the interaction region reach the detector at earlier time as compared to those produced in the field free region. The kinetic energy of a parent ion changes due to a collision. This leads to a distribution in kinetic energy when fragmentation occurs, resulting in a velocity distribution for the neutral fragments, which is reflected in the broadening of the signal observed on detector 1. The kinetic energy release in the fragmentation process is in the order of one electronvolt in the center of mass frame, which is very small as compared to the kinetic energy of the parent in the center of mass (2 or 4 keV).

The laser arrival time is adjusted to select the parent ion. In Figure 2, the red curve is the signal of neutral photofragments recorded when BB^+ ions ($m/z = 156$) are selected, while the blue spectrum corresponds to fragmentation of BBH^+ ions ($m/z = 157$), a typical laser time delay of 100−120 ns being used to select either BB^+ or BBH^+. These signals have been recorded at $\lambda = 460$ nm where both the BB^+ and the BBH^+ are absorbing and shows that the BBH^+ signal is larger than the BB^+ signal. The signal recorded at $m/z = 157$ includes a contribution from the BB^+ isotope with one C^{13} atom, which is 12% of the $m/z = 156$ BB^+ signal, and will thus represent 5% of the signal observed at $m/z = 157$, which is the same order of magnitude as the noise.

When the fragmentation spectrum is recorded, the fluctuation in the discharge source is taken into account by monitoring the collision-induced signal at the same time as the photoinduced signal. The signal from the MCP detectors is sent to the digitizing storage oscilloscope that was interfaced to a PC.

The ions stay in the interaction region for 400 ns, and one can differentiate photofragmentation events that occur in the interaction region or after the interaction region by the arrival time of the fragments on the detector: the fragmentation in the interaction region is the peak at short time, and the signal from fragmentations occurring after the interaction zone should be a narrow peak on top of the broad collision-induced signal (after the interaction region, the kinetic energy of the parent ion is back to 2 keV). Thus, one can get some information on the fragmentation time as it has been shown by recent experiments.[38−40] The time resolution can be improved to 30 ns if the ions are dissociated in an electric field (1 kV/cm) in place of a fixed voltage.[38] In an electric field, the kinetic energy of the parent ion is varying as it travels in the interaction region. Because the velocity of the neutral fragments is the same as that of their parents when fragmentation occurs, the arrival time of the neutrals will be between the narrow peak and the broad peak (Figure 2) and represents a direct measurement of the time at which the fragmentation occurs.

It is clear that the experimental method presented here is not so commonly used among people working with ions. This method is efficient to investigate the absorption spectroscopy of ions using the photodissociation technique because it always produces a neutral fragment independent of the branching ratio. The major drawback

(38) Lucas, B.; Barat, M.; Fayeton, J. A.; Jouvet, C.; Carcabal, P.; Gregoire, G. *Chem. Phys.* **2008**, *347*, 324–330.
(39) Lucas, B.; Barat, M.; Fayeton, J. A.; Perot, M.; Jouvet, C.; Gregoire, G.; Nielsen, S. B. *J. Chem. Phys.* **2008**, *128*, 164302.
(40) Lepere, V.; Lucas, B.; Barat, M.; Fayeton, J. A.; Picard, Y. J.; Jouvet, C.; Carcabal, P.; Nielsen, I.; Dedonder-Lardeux, C.; Gregoire, G.; Fujii, A. *Phys. Chem. Chem. Phys.* **2007**, *9*, 5330–5334.

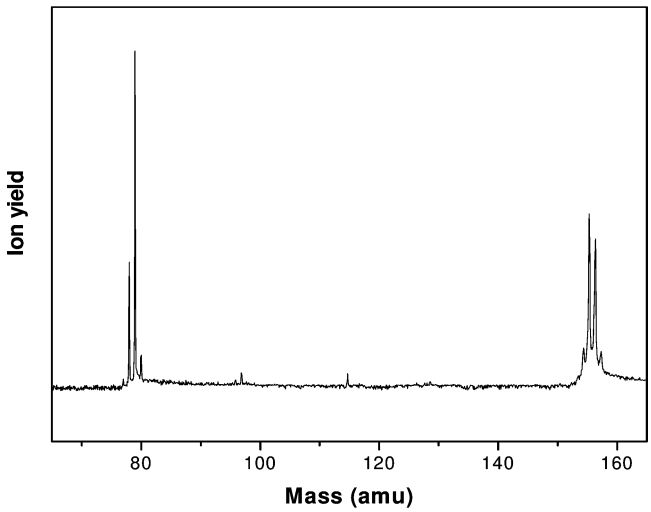

Figure 3. TOF mass spectrum obtained by the discharge source coupled with a supersonic jet for a gas mixture of helium and hydrogen seeded with benzene vapor.

is that there is no information on this branching ratio of the fragmentation process.

Calculations

Ab initio calculations for protonated benzene dimer have been performed with the TURBOMOLE program package,[41] making use of the resolution-of-the-identity (RI) approximation for the evaluation of the electron-repulsion integrals.[42] The equilibrium geometry of the protonated benzene dimer in its closed-shell singlet ground electronic state (S_0) has been determined with the MP2 method. Excitation energies and equilibrium geometry of the lowest excited singlet state have been determined at the CC2 level, making use of the recently implemented CC2 analytic gradients.[43−45] All calculations were performed with the correlation-consistent polarized valence double-ζ (cc-pVDZ),[46] with some comparison with the TZVP basis set. The basis set superposition error (BSSE) is obtained using the counterpoise method.[47]

Results and Discussion

The BBH^+ and BB^+ ions were observed in the mass spectrum of cold molecular beam produced by discharge ion source. The mass spectra were recorded under different stagnation pressures, different discharge condition, and with different concentration of hydrogen to optimize the conditions. A typical mass spectrum obtained at 2 bar backing pressure with 50% hydrogen in helium is presented in Figure 3. The main features observed in the time-of-flight mass spectrum are the benzene ($m/z = 78$), protonated benzene ($m/z = 79$), protonated benzene with C^{13} isotope ($m/z = 80$), BB^+ ($m/z = 156$), BBH^+ ($m/z = 157$), BBH^+ with C^{13} isotope ($m/z = 158$), and higher order clusters.

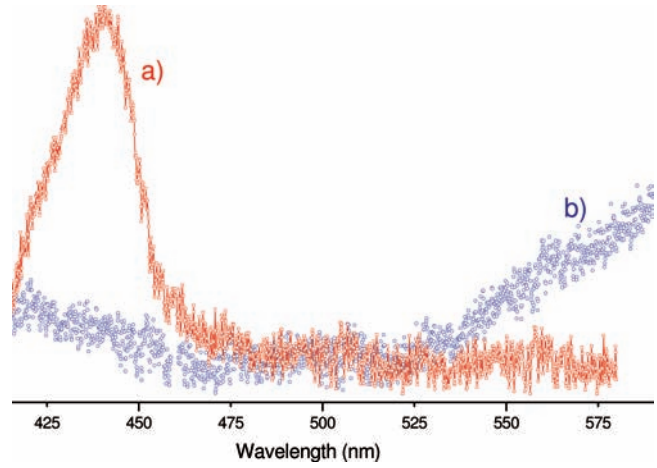

Figure 4. Photodissociation spectra recorded in the 415−600 nm wavelength range: (a) in red, photofragmentation spectrum of protonated benzene dimer BBH^+; and (b) in blue, photofragmentation spectrum of the radical cation BB^+ presented for comparison. This spectrum is very similar to that published by Nakai et al.[37]

We report the photodissociation spectra of BB^+ and BBH^+ in the wavelength range of 415−600 nm (Figure 4) by detecting the neutral fragments. The photodissociation spectrum of BB^+ in the wavelength range of 400−670 nm has already been reported by Nakai et al.[37] The spectrum consists of two local excitation (LE) bands at 430 and 580 nm. These bands are due to the $\pi \leftarrow \pi$ and $\pi \leftarrow \sigma$ transitions of a monomer ion subunit within $(C_6H_6)_2^+$, respectively. The recorded photodissociation spectrum represented in Figure 4b looks very similar to the spectrum reported earlier in this wavelength range, with two broad local excitation bands observed for BB^+.

The photodissociation spectrum of BBH^+ recorded in the same wavelength range using the OPO laser (Figure 4a) shows a marked difference as compared to the BB^+ excitation spectrum. The excitation spectrum of BBH^+ displays only one broad absorption band in the 415−475 nm spectral range. We have scanned up to 670 nm in the lower energy side but could not observe any more absorption.

As it can be seen in Figure 4a, no vibrational progression is observed. One reason could be the insufficient cooling of the sample. The possibility of a contribution from hot bands to the congestion of the spectrum was checked by repeating the experiment at different backing pressures (from 0.5 to 4 bar), gas composition (He/H_2 50/50 or Ar/H_2 50/50), and we could not see any structured band. In similar experimental conditions (1.5 bar, He/H_2, 50/50), protonated benzaldehyde and its complex with water have been observed with structured vibronic bands of widths smaller than 10 cm^{-1}.

It is however difficult to ascertain whether the spectral congestion is intrinsic of the system or is due to temperature. The simultaneous excitation of different ground-state isomers of BBH^+ could also be a reason for this structureless spectral behavior.

The contribution from the fragmentation of higher order clusters into the dimer mass channel can be ruled out because their arrival time into the interaction region with respect to the laser is so different from that of BB^+ or BBH^+ that they cannot be excited simultaneously with the laser.

The fragmentation has also been realized in an electric field for both the BBH^+ and the BB^+ ions in the 460 nm

(41) Ahlrichs, R.; Bar, M.; Haser, M.; Horn, H.; Kolmel, C. *Chem. Phys. Lett.* **1989**, *162*, 165–169.
(42) Weigend, F.; Haser, M. *Theor. Chem. Acc.* **1997**, *97*, 331–340.
(43) Christiansen, O.; Koch, H.; Jorgensen, P. *Chem. Phys. Lett.* **1995**, *243*, 409–418.
(44) Hättig, C.; Weigend, F. *J. Chem. Phys.* **2000**, *113*, 5154–5161.
(45) Köhn, A.; Hättig, C. *J. Chem. Phys.* **2003**, *119*, 5021–5036.
(46) Dunning, T. H. *J. Chem. Phys.* **1989**, *90*, 1007–1023.
(47) Boys, S. F.; Bernardi, F. *Mol. Phys.* **1970**, *19*, 553.

spectral region. No significant broadening of the temporal width of the neutral peak is observed on the detector, which sets an upper limit of the fragmentation time of a few tens of nanoseconds. Because our detection depends on the fragmentation of the ion, the absence of signal below 475 nm for BBH^+ could have been interpreted as the energetical threshold for fragmentation, but in that case the fragmentation time should be very long just above threshold, and because we have not noticed any lengthening of the fragmentation time, we believe that the fragmentation threshold is at lower energy.

BBH^+ is iso-electronic with the neutral benzene dimer. The neutral benzene dimer excitation spectrum obtained by laser-induced fluorescence or REMPI measurement is found to be well resolved, starting at 262.8 nm (4.72 eV) in the UV region close to the benzene transition.[25−28,30,33] The addition of a proton to one of the benzene molecules has a dramatic effect in the excitation spectrum, the S_1-S_0 excitation energy being significantly red-shifted to about 450 nm for BBH^+.

The photofragmentation spectrum observed here can be compared to the photofragmentation of protonated benzene reported by Freiser and Beauchamp[12] that shows a first absorption band with an onset at 380 nm and a maximum at 330 nm. If we compare the onsets of the absorption bands, complexation of protonated benzene with a benzene molecule thus leads to a red shift of 0.7 eV.

To understand this important red shift in the electronic transition of the protonated benzene dimer, calculations on the geometry and energies of the ground and excited states have been performed.

The geometry and binding energy of BB^+ have been reported by several groups.[37,48−51] BB^+ can form different isomers, sandwich, distorted sandwich (parallel displaced), or T-shaped structures. High level theoretical calculation and experimental findings predict that the sandwich geometry is the global minima of the ground state for BB^+.[52,53]

In this study, we have carried out ab initio calculations to find out the geometry and stability of the different possible conformers of BBH^+. The geometry of the most stable complex obtained with RI-MP2/cc-pVDZ level of theory is shown in Figure 5a. It is a parallel displaced structure where the proton is bond to one of the benzene molecules with a bond length only 0.1 Å longer than a usual CH bond. In this geometry, the two benzene molecules remain planar (or almost planar).

We tried to optimize proton bond structures in fixing the proton at equal distance between two carbon atoms of the two benzene molecules, but the structures obtained are much higher in energy (0.3 eV) and are not stable minima. When the constraints are released to reoptimize the system, these structures evolve to the most stable geometry of Figure 5a.

Two T-shaped structures have been calculated (Figure 5c and d), one in which the hydrogens (proton) are pointing toward carbon atoms of the ring, and one in which BH^+ is rotated by 30° along the benzene C_6 axis, the proton pointing between two carbon atoms. These two T-shaped isomers have the same energy (less than 10^{-4} eV energy difference) and are slightly higher in energy ($\Delta E = 0.04$ eV in MP2/cc-pVDZ and 0.08 eV in MP2/TZVP) than the most stable structure. We thus cannot neglect the contribution of the T-shaped structure of BBH^+ to the broad absorption band observed.

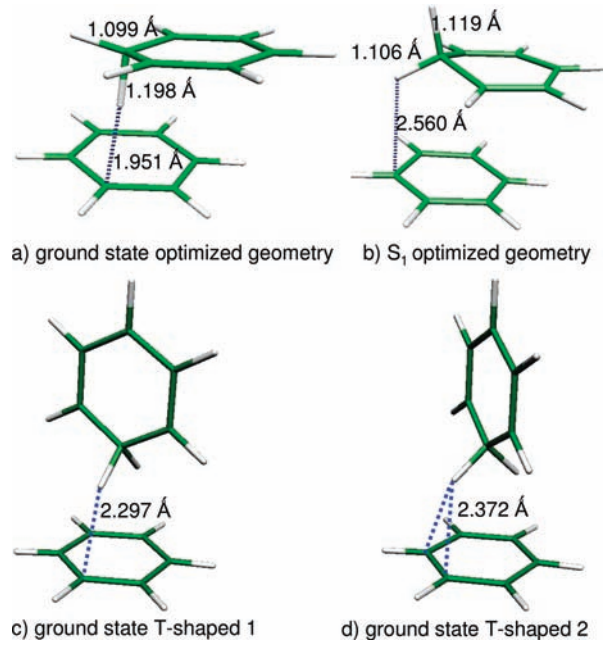

Figure 5. BBH^+-optimized geometry: (a) ground-state geometry (RI-MP2/cc-pVDZ) of the most stable isomer; (b) first excited-state geometry obtained at the RI-CC2/cc-pVDZ level of theory; and (c) and (d) ground-state T-shaped isomers (RI-MP2/cc-pVDZ).

Table 1. Energy and Oscillator Strength for the Ground and First Excited States of the Most Stable Isomer of Protonated Benzene Dimer[a]

protonated benzene dimer BBH^+, parallel displaced isomer				
	energy (eV)	vertical transition energy	oscillator strength	orbitals
Ground-State-Optimized Geometry				
S0	0			
S1	3.61	3.61	0.2441	$\pi1(B)-\pi^*(BH^+)$
S2	3.76	3.76	0.0122	$\pi2(B)-\pi^*(BH^+)$
S3	4.48	4.48	0.0767	$\pi(BH^+)-\pi^*(BH^+)$
S1-Optimized Geometry				
S0	0.75			
S1	2.29	1.54		$\pi1(B)-\pi^*(BH^+)$
S2	3.16	2.41		$\pi2(B)-\pi^*(BH^+)$

[a] All of the energies are scaled with respect to the optimized ground-state energy.

The binding energy of the most stable isomer of BBH^+, calculated at the MP2 level of theory with the cc-pVDZ basis set, including ZPE and BBSE corrections, amounts to 0.49 eV in the ground state, in good agreement with the experimental value reported in the literature.[51]

The vertical transition energies for the lowest BBH^+ excited states have been computed at the RI-CC2 level of theory starting from the ground-state geometry and are listed in Table 1.

The first and second excited states correspond to charge transfer states where an electron of a π orbital (HOMO orbital

(48) Rusyniak, M.; Ibrahim, Y.; Alsharaeh, E.; Mautner, M. M.-N.; El-Shall, M. S. *J. Phys. Chem. A* **2003**, *107*, 7656–7666.
(49) Hiraoka, K.; Fujimaki, S.; Aruga, K. *J. Chem. Phys.* **1991**, *95*, 8413–8418.
(50) Grover, J. R.; Waiters, E. A.; Huit, E. T. *J. Phys. Chem.* **1987**, *91*, 3233–3237.
(51) Meot-Ner, M.; Hamlet, P.; Hunter, E. P.; Field, F. H. *J. Am. Chem. Soc.* **1978**, *100*, 5466.
(52) Bouvier, B.; Brenner, V.; Millie, P.; Soudan, J.-M. *J. Phys. Chem. A* **2002**, *106*, 10326–10341.
(53) Rusyniak, M. J.; Ibrahim, Y. M.; Wright, D. L.; Khanna, S. N.; El-Shall, M. S. *J. Am. Chem. Soc.* **2003**, *125*, 12001–12013.

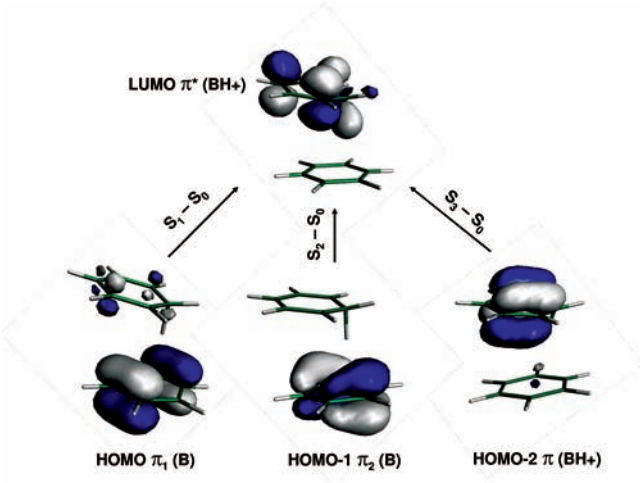

Figure 6. Scheme of the molecular orbitals involved in the lowest electronic transitions of BBH^+.

for S_1 and HOMO−1 orbital for S_2) localized on the neutral benzene molecule is promoted to the LUMO π^* orbital localized on the protonated benzene moiety (Figure 6). The calculated vertical transition energy in BBH^+ is found to be around 3.61 eV (344 nm). It is a very strong transition with oscillator strength of 0.24. The third excited state is a $\pi\pi^*$ transition on the protonated benzene moiety, located in the UV (4.48 eV) slightly red-shifted as compared to the S_1-S_0 transition in neutral benzene dimer (4.72 eV).

The first excited-state geometry has also been optimized starting from the ground-state geometry, and a significant change, shown in Figure 5b, is obtained. The aromatic ring containing the proton has become significantly nonplanar in the S_1 state, the carbon atom bearing the charge comes out of plane, while the 2 CH bonds become almost equal in length. With this geometry, the stabilization energy of the excited state is 1.3 eV leading to a transition at 1.54 eV, the ground-state energy of the complex obtained at the optimized excited-state geometry being 0.75 eV higher in energy than the global minimum structure.

Recent calculations performed on the protonated benzene monomer[54] have shown that the first excited state is a $\pi\pi^*$ transition in the UV region calculated at 4.07 eV. The first excited-state geometry optimization leads to ring deformation and probably causes a fast internal conversion toward the ground state through a conical intersection. The deformation of the aromatic ring in the excited state of the protonated benzene monomer is even greater than in the protonated dimer: in the protonated monomer, the dihedral deformation of the ring is around 40°, whereas in the dimer it is only 12°; the presence of the other benzene molecule nearby the protonated ion reduces the excited-state deformation. The corresponding $\pi\pi^*$ transition in the protonated dimer, localized on the protonated part, is the S_3 transition calculated at 4.48 eV: thus the presence of neutral molecule near the protonated benzene ion seems to destabilize this $\pi\pi^*$ excited state.

The T-shaped isomers despite a very different structure have electronic properties similar to those of the most stable isomer. Because the two structures shown in Figure 5c and d have very similar energies, only the excited-state energies of isomer 1 have been calculated. The vertical transition energies as well as the first excited-state-optimized energy (calculated at the same level of theory RI-CC2/cc-pVDZ) are listed in Table 2. The excited-state optimization has been performed, and the major change is an increased distance between the two molecules. The distance between the proton of BH^+ and the nearest carbon atom in benzene changes from 2.297 to 3.368 Å.

Table 2. Energy and Oscillator Strength for the Ground and First Excited States of the T-Shaped Isomer of Protonated Benzene Dimer[a]

protonated benzene dimer BBH^+, T-shaped isomer 1				
	energy (eV)	vertical transition energy (eV)	oscillator strength	orbitals
Ground-State-Optimized Geometry				
S0	0	0		
S1	3.41	3.41	0.2538	$\pi1(B)-\pi^*(BH^+)$
S2	3.46	3.46	0.0000	$\pi2(B)-\pi^*(BH^+)$
S3	4.18	4.18	0.1056	$\pi(BH^+)-\pi^*(BH^+)$
S1-Optimized Geometry				
S0	0.5			
S1	2.36	1.86		$\pi1(B)-\pi^*(BH^+)$
S2	2.79	2.41		$\pi2(B)-\pi^*(BH^+)$

[a] This isomer is 0.04 eV higher in energy than the parallel displaced isomer at the MP2/cc-pVDZ level of theory. All of the energies are scaled with respect to the T-shaped-optimized ground-state energy.

The S_0-S_1 vertical excitation of T-shaped isomer is slightly lower in energy (0.2 eV) as compared to the parallel displaced isomer, and the important point is that the first excited states also correspond to charge transfer states where an electron initially localized on the neutral benzene molecule is promoted to the protonated benzene moiety. As in the most stable isomer, the locally excited $\pi\pi^*$ state is higher in energy (4.18 eV). Optimization of the excited-state geometry leads to a strong stabilization of the excited state by 1.1 eV, and the optimized energy is 2.36 eV, very close to the optimized S_1 energy of the parallel-displaced isomer. Thus, excitation of the T-shaped isomer is also compatible with the observed unresolved excitation spectrum.

The observed transition presents a broad absorption in the range of 415−475 nm, between the calculated adiabatic and vertical transition, with a slow rising edge. The calculation shows that a large change in geometry occurs between the optimized ground-state structure and the optimized excited state for both isomers. The 0−0 transition probably cannot be excited, and the Franck−Condon factors should be large enough only for high vibrational levels. This system being a cluster, low frequency modes are present and the density of levels should be quite large in the Franck−Condon accessible region, and thus the spectrum should probably be intrinsically congested.

It should be emphasized that the first transitions in the BB^+ radical cations have a different character than the transitions in BBH^+. The radical cation has an open shell electronic structure, and the lowest transitions involve promotion of an electron from lower orbitals (σ or π) to the half empty HOMO orbital (π), these transitions being close to the (B−X and C−X) transitions of the benzene monomer cation (red-shifted only by 0.2 eV).[55] Conversely, BBH^+ is a closed shell electronic species, which should resemble the

(54) Rode, M. F.; Sobolewski, A. L.; Dedonder-Lardeux, C.; Jouvet, C.; Dopfer, O. *J. Phys. Chem. A* **2009**, *113*, 5865–5873.

(55) Ohashi, K.; Nishi, N. *J. Chem. Phys.* **1991**, *95*, 4002–4009.

neutral cluster. For the parallel displaced and the T-shaped isomers, the two lowest excited states are charge transfer states, which are calculated ~0.8 eV lower than the local excitation. These states are specific of the protonated dimer species. The charge transfer state correlates at large distance to a dissociation limit in $BH^{\bullet} + B^{+}$, while the BBH^{+} ground state correlates to $BH^{+} + B$. The relative energies of these dissociation limits can be evaluated from the ionization potential of B (9.24 eV) and the $BH^{\bullet}$ ionization potential that has been calculated here to be 5.9 eV, which places the excited-state dissociation limit 3.34 eV above the ground-state dissociation limit. The ground-state binding energy being 0.65 eV (without ZPE and BSSE corrections) and the transition energy at 2.29 eV, the binding energy of the charge transfer state is 1.70 eV, much larger than the ground-state binding energy.

It should be noted that the BBH^{+} absorption seems analogous to the visible absorption (in the 420−550 nm range) of the excimer state of the benzene dimer evidenced by Saigusa et al.[33,56] and assigned to transition from the excimer state to a charge transfer state. In the neutral benzene dimer, the visible absorption corresponds to a transition in the excited-state manifold, while in BBH^{+} the visible absorption starts from the ground state.

(56) Saigusa, H.; Morohoshi, M.; Tsuchiya, S. *J. Phys. Chem. A* **2001**, *105*, 7334–7340.

Conclusion

The first transition in the protonated benzene dimer is observed around 450 nm and is largely red-shifted in comparison with the neutral dimer (isoelectronic) transition. This transition is also strongly red-shifted with respect to the protonated benzene transition.[12] This effect is due to the charge transfer character of the first excited state, where an electron of the π orbital localized on the neutral benzene moiety is transferred to a π^* orbital on the protonated benzene part.

Acknowledgment. This work has been supported by the Université Paris-Sud 11 (PPF Applications of lasers in physico-chemistry and biomedical photonics), by the ANR research grant (NT05-1 44224), and by the PROCOPE 17832NK program. I.B.N. thanks the FNU (Forskningsrådet for Natur og Univers) for funding. We are greatly indebted to Prof. O. Dopfer for helpful discussions and suggestions. R.O. thanks the Isfahan University of Technology for financial support.

JA903181K